Formation and Structure of Graphene Waves on Fe(110)

Vinogradov, Nikolay; Zakharov, Alexei; Kocevski, V.; Rusz, J.; Simonov, K. A.; Eriksson, O.; Mikkelsen, Anders; Lundgren, Edvin; Vinogradov, A. S.; Mårtensson, Nils; Preobrajenski, Alexei

[Link to publication]

Formation and Structure of Graphene Waves on Fe(110)

N. A. Vinogradov,[1,2] A. A. Zakharov,[2] V. Kocevski,[1] J. Rusz,[1] K. A. Simonov,[3] O. Eriksson,[1] A. Mikkelsen,[4]
E. Lundgren,[4] A. S. Vinogradov,[3] N. Mårtensson,[1,2] and A. B. Preobrajenski[2,*]

[1]*Department of Physics and Astronomy, Uppsala University, Box 530, 75121 Uppsala, Sweden*
[2]*MAX-lab, Lund University, Box 118, 22100 Lund, Sweden*
[3]*V.A. Fock Institute of Physics, Saint-Petersburg State University, 198504, Saint-Petersburg, Russia*
[4]*Division of Synchrotron Radiation, Institute of Physics, Lund University, Box 118, 22100 Lund, Sweden*
(Received 8 February 2012; published 9 July 2012)

A very rich Fe-C phase diagram makes the formation of graphene on iron surfaces a challenging task. Here we demonstrate that the growth of graphene on epitaxial iron films can be realized by chemical vapor deposition at relatively low temperatures, and that the formation of carbides can be avoided in excess of the carbon-containing precursors. The resulting graphene monolayer creates a novel periodically corrugated pattern on Fe(110). Using low-energy electron microscopy and scanning tunneling microscopy, we show that it is modulated in one dimension forming long waves with a period of ~4 nm parallel to the [001] direction of the substrate, with an additional height modulation along the wave crests. The observed topography of the graphene/Fe superstructure is well reproduced by density functional theory calculations, and found to result from a unique combination of the lattice mismatch and strong interfacial interaction, as probed by core-level photoemission and x-ray absorption spectroscopy.

One of the major routes for producing high-quality monolayer graphite (MG or graphene) on a large scale is the use of metal substrates as a support for its growth [1]. On close-packed 3d metal surfaces graphene can grow in a lattice-matched fashion, e.g., on Ni(111) [2–6] and Co(0001) [7,8], where it is strongly bonded to the substrate due to the metal $3d$-C$2p(\pi)$ orbital mixing, or on Cu(111) [9], where graphene is weakly physisorbed because the Cu 3d states are fully occupied and pushed down from the Fermi level. Altogether, nearly flat epitaxial graphene monolayers of high structural quality can be formed on all these substrates. In contrast, on the close-packed surfaces of 4d and 5d transition metals graphene monolayer is lattice-mismatched resulting in a variety of moiré superstructures and associated with them geometrical corrugations. Symmetry and periodicity of the corrugation are dictated by the lattice mismatch, while the corrugation amplitude and the average carbon-to-substrate distance are defined by the strength of metal $4(5)d$-C$2p\pi$ chemical interaction. Different structures were found for graphene adsorbed on Pt(111) [10–12], Ir(111) [11,13–15], Rh(111) [11,16] and Ru(0001) [11,17–19]. While on Pt(111) graphene can be considered quasifreestanding and shows almost no corrugation due to the weak interaction with the substrate, it is slightly buckled on Ir(111) and strongly corrugated on Rh(111) and Ru(0001) [11]. Corrugated graphene monolayers were shown to be robust and versatile templates for self-assembly of metal clusters, nanoparticles, etc., in 2D arrays [16,20–22].

It is remarkable in this context that the interface between graphene and the most widespread transition metal, iron, has not been studied in detail yet. The main reason for this is probably the challenging procedure of graphene growth. In the Fe-C phase diagram the separation of phases into bcc-iron and graphite is suppressed because of the preferential nucleation of the metastable Fe_3C phase [23]. Therefore, the very possibility of growing graphene on top of a Fe film is *a priori* not evident, because the formation of different combinations of bcc- and fcc-iron with iron carbide (cementite, Fe_3C) is thermodynamically favorable. From a practical point of view, the technology of graphene growth on Fe films is very attractive because of the considerable price reduction in comparison with using other transition metal substrates. A recent report from Fujitsu Laboratories demonstrated a potential of Fe catalyst films for production of multilayer graphene for top-gated field effect transistors [24].

Provided a single monolayer of graphene can indeed be grown on a surface of bcc Fe, its morphology is expected to be very different from the nearly flat sheets formed on the close-packed surfaces of other 3d metals, because none of the Fe faces is lattice-matched to graphene in two dimensions. On the other hand, graphene is expected to interact strongly with Fe (by analogy with Ni and Co), and the shortest Fe-Fe distance (0.248 nm) is close to the lattice constant in graphene (0.246 nm). In this connection, the Fe(110) face with its distorted hexagonal symmetry is a good candidate for new types of graphene nanopatterning, e.g., striped corrugation patterns, because of a partial match to the graphene lattice.

In this Letter we demonstrate that it is possible to grow high-quality single-layer graphene on the Fe(110) substrate by fine tuning the conventional CVD process and by going beyond the conditions of thermodynamical equilibrium.

By a combination of several experimental techniques and theoretical calculations we show that graphene on Fe(110) represents a complex surface superstructure and determine its periodicity, corrugation, and the nature of interaction between graphene and the substrate. Based on the experimental results and DFT we suggest an atomic model for the graphene/Fe(110) interface.

The core-level spectroscopy (PES and NEXAFS) and the μLEED/LEEM experiments were performed at the MAX-lab beam lines D1011 and I311, while STM studies were performed in a separate chamber. Fe films with the (110) orientation and the thickness of ~ 20 nm were grown epitaxially on the W(110) surface precleaned in UHV. The MG samples were prepared by thermal decomposition of the C_3H_6 gas at temperatures between 520 and 600 °C in the gas pressure of 2–4×10^{-6} mbar for ~ 200 s. At 520 °C the C_3H_6 pressure corresponding to an equilibrium between the number of deposited and reevaporated C atoms is around 1×10^{-8} mbar, but only the iron carbide phase formation has been observed at this low pressure. When the hydrocarbon gas pressure was kept in the range of 10^{-7} mbar (in the same temperature range), a mixture of carbide and graphene was typically observed. Therefore, highly nonequilibrium growth conditions with excess of carbon are essential to suppress the formation of Fe carbide in favor of graphene growth.

The carbide and graphene phases can be clearly distinguished in low-energy electron microscopy (LEEM). In Fig. 1(a) a LEEM image recorded in the tilted bright-field mode clearly shows two domains of iron carbide on Fe(110) aligned preferably along the step edges, with the characteristic μLEED patterns from each domain shown in Fig. 1(c) and 1(d). The principle spots from Fe(110) are marked by yellow circles, and a carbide-induced (16×4) reconstruction is visible. It can be associated with a thin cementite film matched to Fe(110) with the $Fe_3C(100)$ face. In this case the two observed domains may result from aligning the [010] direction in cementite parallel to either [$1\bar{1}1$] or [$\bar{1}11$] in bcc Fe.

In contrast to carbide, graphene on Fe(110) always forms only one domain, as visible from the LEEM image in Fig. 1(b) showing a uniform coverage of the iron surface with a graphene monolayer. Because of the carbon solubility in iron, graphene bi- and trilayers can be grown too by adjusting the growth parameters, but they are not discussed further in this Letter. The dark elongated features are due to the large-scale defects (cracks) developed in the Fe film upon annealing. The μLEED from MG/Fe(110) [Fig. 1(f)] demonstrates a complex moiré pattern, and is identical with the macro-LEED pattern (not shown). The principal spots from the iron substrate (marked by yellow circles) are accompanied by the principal spots from graphene (blue circles) and a number of satellite spots due to the formation of a superstructure. On under-annealed samples, characteristic segmented circles from misoriented
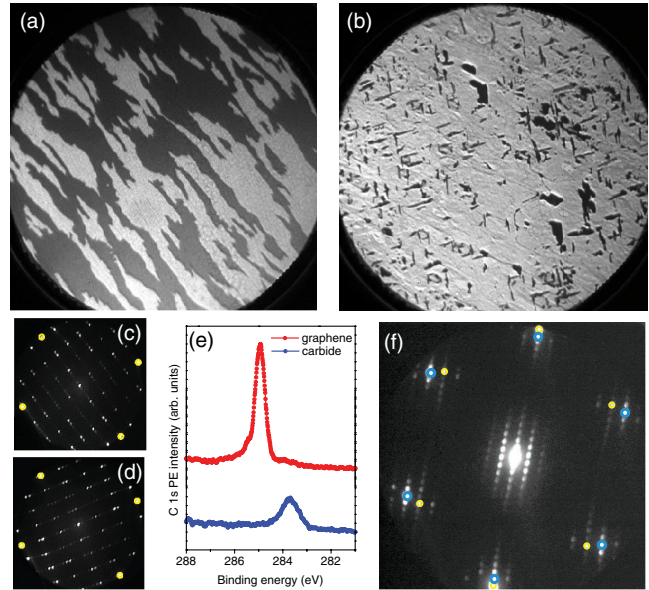

FIG. 1 (color online). LEEM images of (a) iron carbide ($E = 3.5$ eV) and (b) graphene ($E = 4.6$ eV) grown on Fe(110); field of view 15 μm. (c) and (d) μLEED patterns from two equivalent carbide domains ($E = 30$ eV). (e) C 1s μXPS from (a) and (b). (f) μLEED pattern from graphene on Fe(110) ($E = 52$ eV) (slightly elongated due to lens distortions in the microscope); principle spots from graphene are outlined in blue; principal spots from the Fe(110) substrate are marked yellow.

graphene flakes can additionally be seen in LEED. From the spot positions the periodicity of the supercell is derived as (6×18) in terms of the Fe(110) unit cell, or (7×17) if graphene hexagons are used as structural units. This means that 7 graphene rings in the zigzag direction match 6 Fe-Fe distances in the [001] direction on Fe(110), and 17 graphene rings in the armchair direction match 18 Fe rows in the [$1\bar{1}0$] direction on Fe(110). The chemical contrast between carbide and graphene is reflected in a large binding energy shift (~ 1.3 eV) and different shape of the C 1s photoemission line, as shown in Fig. 1(e).

The large-scale real-space structure of graphene on Fe(110) is shown in the overview STM image [Fig. 2(a)]. The surface is covered by graphene completely, except the patches of a disordered phase (denoted **A** on the image) with the areal fraction of 5 to 10%, which can be associated with the dark protrusions observed by LEEM [Fig. 1(b)]. The moiré superstructure attributed to the MG/Fe(110) interface appears in the overview STM images as long equidistant stripes with a periodicity of ~ 4 nm. Zooming on these stripes [Fig. 2(b)] allows us to estimate the corrugation amplitude perpendicular to them as $\sim 0.6 \pm 0.2$ Å (based on analysis of many images). A profile of the STM tip height along the green line across the stripes is depicted in Fig. 2(c), and a simple sinusoidal fit serves as a guide to the eye (note that the real profile has a more complicated

FIG. 3 (color online).   (a) Positions of the C atoms in graphene on Fe(110) calculated by DFT, with the colormap representing the magnitude of corrugation. (b) calculated vertical position of the STM tip above the MG/Fe(110) surface supercell obtained from an isosurface of the LDOS with value 10^{-5} states/(a.u.)^3 and an energy range from -0.05 eV to $+0.05$ eV.
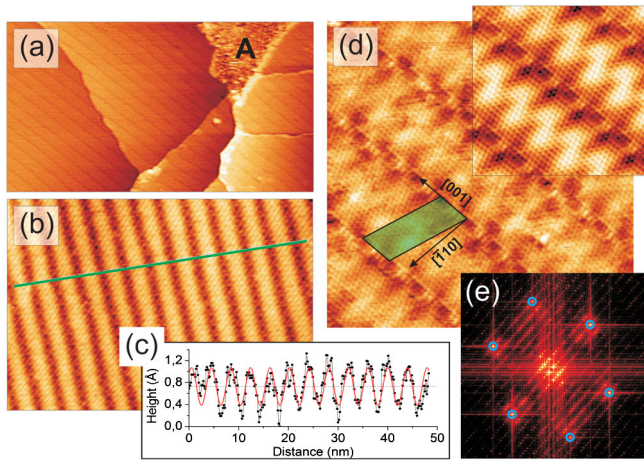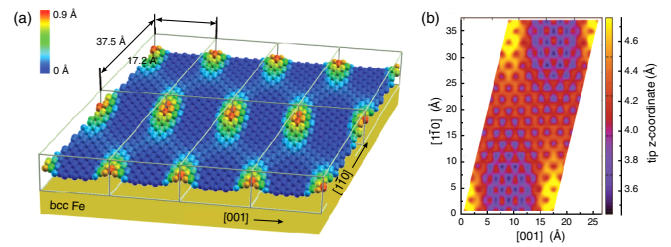
FIG. 2 (color online).   (a) Overview STM image of graphene on Fe(110) with a characteristic striped corrugation pattern. A small patch of disordered phase is denoted with **A**. Scan length is 115 nm, $I_t = 0.5$ nA, $V_b = -0.015$ V. (b) STM image of graphene waves (length 50 nm, $I_t = 1$ nA, $V_b = 0.005$ V) with (c) height profile along the straight line drawn in (b). (d) Close-up STM image taken from the area in (a) marked with a square. Scan size is 15×15 nm, $I_t = 1.2$ nA, $V_b = 0.012$ V. The surface supercell is indicated, while inset in the top-right corner demonstrates the very same part of the image averaged over the supercell. (e) Fast Fourier transform from (d) after averaging; principle graphene spots are marked with blue circles.

shape). The image in Fig. 2(d) provides insight into the atomic structure of graphene/Fe(110) by zooming on the area marked with a square in Fig. 2(a). In this image individual graphene rings are clearly visible, with the hexagonally arranged dips attributed to the centers of the rings and honeycomb-shaped bright protrusions associated with the electron density centered on C atoms. The surface supercell deduced from our μLEED/LEEM studies is marked on Fig. 2(d), while the top-right inset in the panel shows the very same patch of the scan, averaged over the depicted supercell. To emphasize the agreement between the STM and μLEED/LEEM results, we show in Fig. 2(e) a fast Fourier transform (FFT) from the supercell-averaged image in Fig. 2(d). The FFT image is very similar to the μLEED pattern in Fig. 1(b) implying the long-range structure of the MG/Fe(110) interface is preserved on the nanometer scale. Thus, the sample surface is covered with a graphene monolayer, which shows a complex moiré superstructure and is significantly corrugated. Interestingly, a monolayer of hexagonal BN (which is isostructural and isoelectronic to graphene) can also be grown on Fe(110), but it forms two distinct domains with a very different surface reconstruction due to inequivalent bonding of the B and N sublattices to iron [25].

The detailed atomic structure of the MG/Fe(110) interface has been studied with the spin-polarized ground-state density functional theory (DFT) calculations. The calculations were performed using LDA exchange-correlation

potential with SIESTA pseudopotential package [26,27] with the basis-set setup DZP for iron and DZ for carbon. We have optimized the MG/Fe(110) structure by calculation of forces acting on atoms until those are converged below 0.05 eV/Å. We set up a simulation cell consisting of 6 flat layers of iron and added graphene on top of it, which initially was flat. In the first step of relaxation only a z coordinate of carbon was allowed to relax. After that converged, the positions of all C atoms and the Fe atoms in the two topmost substrate layers were allowed to relax in all coordinates. The geometrical interface relief in the calculated MG/Fe(110) system is strongly corrugated [Fig. 3(a)]. The distances of the graphene monolayer from the average z-coordinate of the topmost Fe layer are 2.12 Å (minimal), 3.03 Å (maximal), and 2.32 Å (average), resulting in the overall corrugation amplitude of ~0.9 Å. The topmost Fe layer is also slightly buckled following the corrugation of graphene, although with a reduced amplitude of 0.18 Å. Of 238 C atoms in the supercell only a small fraction is considerably elevated over the Fe surface: 20 atoms are above 2.7 Å, 8 atoms are above 2.9 Å. They are hardly visible on the overview STM images resulting in a somewhat smaller experimental corrugation, which is only 0.6 ± 0.2 Å perpendicular to the graphene waves (i.e., perpendicular to the [001] direction of the substrate). The distances around 2.7 Å are too short for breaking the C-Fe covalent bonds, and the entire graphene film is strongly interacting with the substrate. In Fig. 3(b) a calculated STM image is plotted using the Tersoff-Hamann approximation. The range of the local density of states (LDOS) was set to ± 0.05 eV around the Fermi level. The plot shows a map of the tip z coordinate, at which LDOS has a constant value of 10^{-5} states/(a.u.)^3. The range of z values is consistent with the calculated corrugation of the graphene layer; it agrees qualitatively with the observed STM patterns in Fig. 2(b). On the whole, we suggest that the real geometrical corrugation of graphene on Fe(110) lies between the STM value of 0.6 Å and the DFT value of 0.9 Å. Note that the LDA may be a source of some inaccuracy in our calculations. Improved exchange-correlation functionals, e.g., those including
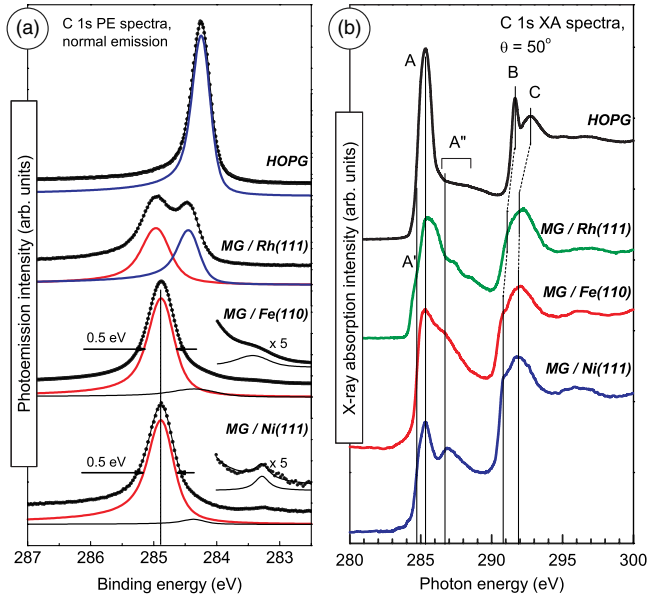
FIG. 4 (color online). (a) C 1*s* photoelectron spectra from graphene on Fe(110) compared with those from graphene on Rh(0001) and Ni(111), and from HOPG. Photon energy is 350 eV; (b) C 1*s* NEXAFS spectra from the same systems. θ is the angle between the polarization vector of incident radiation and the surface normal.

van der Waals interaction, may further improve the accuracy of the resulting corrugation pattern.

The electronic structure of graphene on Fe(110) has been studied by photoemission and x-ray absorption. The C 1*s* PE spectrum in Fig. 4(a) is dominated by one strong component with the binding energy of 284.9 eV and the full width at half maximum of 0.5 eV, which are the same as for the C 1*s* photoemission spectroscopy (PES) from graphene chemisorbed on the lattice-matched Ni(111) surface, shown here as a reference. This implies that graphene interacts strongly with Fe(110), and its electronic structure is significantly disturbed. The weak component at ~283.4 eV is probably due to a small admixture of carbide, while another weak component at ~284.4 eV may be due to flake edges or Stone-Wales defects in graphene, because its intensity can be reduced by lengthy annealing. This fact correlates with the observation of Stone-Wales defects in graphene grown on Ni(111) at insufficiently high temperatures [28]. In the C 1*s* PE spectrum from strongly corrugated graphene the signal is usually split in two distinct components corresponding to the bonding and nonbonding (elevated) parts of the monolayer, as shown in Fig. 4(a) for graphene on Rh(111) [11]. No such splitting of the C 1*s* core level is observed for graphene on Fe(110). An obvious reason for this is a lack of extended flat regions of graphene lifted significantly above the metal surface, as shown in the DFT calculations above. This implies that the entire monolayer is strongly coupled electronically to the Fe substrate, even at the crests of the stripes.

The C 1*s* NEXAFS spectrum from the MG/Fe(110) system [Fig. 4(b)] is dominated by details A'-A-A'' corresponding to unoccupied states of the π symmetry. In comparison with the C 1*s* NEXAFS spectrum from HOPG, the region of the π states is strongly modified for graphene on Fe(110) due to the pronounced Fe 3*d*-C2*p*(π) orbital hybridization, very similar to the case of graphene chemisorption on Rh(111) [11] and Ni(111) [6]. Also the energy separation between the π (A'-A-A'') and σ (B, C) manifolds in the C 1*s* NEXAFS is reduced in going from HOPG to graphene on Rh, Fe, and Ni, reflecting a weakening of the in-plane σ bonds as a result of this chemisorption. Moreover, this separation is slightly reduced also in going from graphene on Rh to graphene on 3*d* metals, thus suggesting a further increase in the interaction strength. This may explain why the corrugation of graphene is less pronounced on Fe(110) than on Rh(111), and does not result in a double-peak structure in the C 1*s* PES.

In conclusion, we report on the possibility of *in situ* graphene growth on the Fe(110) surface by going beyond the thermodynamic equilibrium conditions during the CVD process to avoid formation of carbide phases. The resultant graphene adlayer demonstrates high structural quality and low defect density. Graphene on Fe(110) is strongly chemisorbed and corrugated in a periodic wavy pattern, with the distance of ~4 nm between the waves and the amplitude between 0.6 and 0.9 Å perpendicular to the waves. A unique combination of the lattice mismatch and strong Fe 3*d*-C2*p*(π) orbital hybridization is responsible for the formation of graphene waves on Fe(110).

*alexeip@maxlab.lu.se

[1] J. Wintterlin and M.-L. Bocquet, Surf. Sci. **603**, 1841 (2009).
[2] Y. Gamo, A. Nagashima, M. Wakabayashi, M. Terai, and C. Oshima, Surf. Sci. **374**, 61 (1997).
[3] G. Bertoni, L. Calmels, A. Altibelli, and V. Serin, Phys. Rev. B **71**, 075402 (2005).
[4] A. Varykhalov, J. Sánchez-Barriga, A. Shikin, C. Biswas, E. Vescovo, A. Rybkin, D. Marchenko, and O. Rader, Phys. Rev. Lett. **101**, 157601 (2008).
[5] A. Grüneis and D. V. Vyalikh, Phys. Rev. B **77**, 193401 (2008).
[6] J. Rusz, A. B. Preobrajenski, M. L. Ng, N. A. Vinogradov, N. Mårtensson, O. Wessely, B. Sanyal, and O. Eriksson, Phys. Rev. B **81**, 073402 (2010).
[7] A. Varykhalov and O. Rader, Phys. Rev. B **80**, 035437 (2009).

[8] D. Eom, D. Prezzi, K. T. Rim, H. Zhou, M. Lefenfeld, S. Xiao, C. Nuckolls, M. S. Hybertsen, T. F. Heinz, and G. W. Flynn, Nano Lett. **9**, 2844 (2009).

[9] L. Gao, J. R. Guest, and N. P. Guisinger, Nano Lett. **10**, 3512 (2010).

[10] T. A. Land, T. Michely, R. J. Behm, J. C. Hemminger, and G. Comsa, Surf. Sci. **264**, 261 (1992).

[11] A. B. Preobrajenski, M. L. Ng, A. S. Vinogradov, and N. Mårtensson, Phys. Rev. B **78**, 073401 (2008).

[12] P. Sutter, J. T. Sadowski, and E. Sutter, Phys. Rev. B **80**, 245411 (2009).

[13] J. Coraux, A. T. N'Diaye, C. Busse, and T. Michely, Nano Lett. **8**, 565 (2008).

[14] J. Coraux, A. T. N'Diaye, M. Engler, C. Busse, D. Wall, N. Buckanie, F. J. M. zu Heringdorf, R. van Gastel, B. Poelsema, and T. Michely, New J. Phys. **11**, 039801 (2009).

[15] C. Busse, P. Lazić, R. Djemour, J. Coraux, T. Gerber, N. Atodiresei, V. Caciuc, R. Brako, A. T. N'Diaye, S. Blügel *et al.*, Phys. Rev. Lett. **107**, 036101 (2011).

[16] M. Sicot, S. Bouvron, O. Zander, U. Rüdiger, Y. S. Dedkov, and M. Fonin, Appl. Phys. Lett. **96**, 093115 (2010).

[17] S. Marchini, S. Günther, and J. Wintterlin, Phys. Rev. B **76**, 075429 (2007).

[18] T. Brugger, S. Günther, J. B. Wang, H. Dil, M.-L. Bocquet, J. Osterwalder, J. Wintterlin, and T. Greber, Phys. Rev. B **79**, 045407 (2009).

[19] P. Sutter, J. Sadowski, and E. A. Sutter, J. Am. Chem. Soc. **132**, 8175 (2010).

[20] A. T. N'Diaye, S. Bleikamp, P. J. Feibelman, and T. Michely, Phys. Rev. Lett. **97**, 215501 (2006).

[21] A. T. N'Diaye, T. Gerber, C. Busse, J. Mysliveček, J. Coraux, and T. Michely, New J. Phys. **11**, 103045 (2009).

[22] E. Sutter, P. Albrecht, B. Wang, M.-L. Bocquet, L. Wu, Y. Zhu, and P. Sutter, Surf. Sci. **605**, 1676 (2011).

[23] H. Okamoto, J. Phase Equilib. **13**, 543 (1992).

[24] D. Kondo, K. Yagi, N. Harada, M. Sato, M. Nihei, S. Sato, and N. Yokoyama, MRS Proc. **1205**, L03 (2009).

[25] N. A. Vinogradov, A. A. Zakharov, M. L. Ng, A. Mikkelsen, E. Lundgren, N. Mårtensson, and A. B. Preobrajenski, Langmuir **28**, 1775 (2012).

[26] P. Ordejón, E. Artacho, and J. M. Soler, Phys. Rev. B **53**, R10441 (1996).

[27] J. M. Soler, E. Artacho, J. D. Gale, A. García, J. Junquera, P. Ordejón, and D. Sánchez-Portal, J. Phys. Condens. Matter **14**, 2745 (2002).

[28] P. Jacobson, B. Stöder, A. Garhofer, G. S. Parkinson, M. Schmid, R. Caudillo, F. Mittendorfer, J. Redinger, and U. Diebold, J. Phys. Chem. Lett. **3**, 136 (2012).